ORIGINAL RESEARCH

Fouling Analysis and the Recovery of Phytosterols from Orange Juice Using Regenerated Cellulose Ultrafiltration Membranes

Nurul Hainiza Abd-Razak[1,2] · M. N. Zairossani[2] · Y. M. John Chew[1] · Michael R. Bird[1]

Abstract

This study describes the use of regenerated cellulose (RCA) membranes with molecular weight cut-off (MWCO) values of 10, 30, and 100 kDa, respectively, to separate phytosterols from orange juice for possible nutraceutical production. A desirable membrane separation rejects protein whilst transmitting phytosterols and other low molecular mass compounds such as sugars. The ultrafiltration was performed in a cross-flow membrane system with a total filtration area of 336 cm^2. Total phytosterol analysis was carried out by using a Liebermann-Buchard-based method. Protein concentration was quantified by the Bradford method. The effects of three different membranes upon the rejection of total phytosterol content, proteins, sugar, and antioxidant activity were studied. Of the membranes tested, the 10-kDa membrane displayed the highest concentration of phytosterols in the permeate. The 30-kDa and 100-kDa membranes gave comparatively higher phytosterol rejection. The membrane surface roughness and corresponding pure water flux values varied as a function of MWCO such that RCA30 > RCA100 > RCA10. Membranes with rougher surfaces displayed higher fouling than those with smoother surfaces. Hydrophobicity and surface roughness both influenced filtration performance, by controlling the development of the protein-based foulant which modified membrane selectivity.

Keywords Fouling · Membrane selectivity · Water flux · Surface roughness · Hydrophobicity

Introduction

Plant sterols, generally known as phytosterols, are cholesterol-like compounds that are found mostly in vegetable oils, nuts, and fruits (Wang et al. 2018). The structure is related to cholesterol but differs in the structure of the side chain. Phytosterols consist of a steroid skeleton with a hydroxyl group attached to the C-3 atom of the A-ring. The most common phytosterols are stigmasterol and β-sitosterol. Commercial phytosterols were isolated mostly from soybean oil. Stigmasterol has a molecular weight of 412 g mol^{-1} with elemental formula $C_{29}H_{48}O$. For β-sitosterol, the elemental formula is $C_{29}H_{50}O$ with a molecular weight of 414 g mol^{-1} (Kongduang et al. 2012; McDonald et al. 2012). Phytosterols

are widely used as food additives due to their ability to lower human cholesterol levels (Marangoni and Poli 2010). Phytosterols are also known for their anticancer properties by inhibiting the progression of the cancer cell cycle (Shahzad et al. 2017). The global market size of phytosterols is expected to increase to USD 1100 million by 2025, from USD 590 million in 2018 (Market-Insights-Reports 2019).

The main limitations concern the lack of techniques that can be used for the economical extraction and separation of phytosterol compounds from various plants. Conventional techniques such as Soxhlet extraction has been used to extract phytosterols from melon seeds (Nyam et al. 2011). Phytosterols from rapeseed were extracted using the microwave extraction technique (Yang et al. 2013). Alternative extraction methods such as supercritical fluid extraction have been used to isolate phytosterols from melon seeds (Nyam et al. 2011). There are some drawbacks associated with these techniques. The use of toxic organic solvents and the use of supercritical fluid that involves high pressures and high temperatures consume large amounts of energy and produce considerable waste, making them costly and unsustainable (Conidi et al. 2017). Membrane separation techniques such

✉ Michael R. Bird
M.R.Bird@bath.ac.uk

[1] Centre of Advanced Separations Engineering, Department of Chemical Engineering, University of Bath, Bath BA2 7AY, UK

[2] Malaysian Rubber Board, Rubber Research Institute of Malaysia, PO Box 10150, 50908 Kuala Lumpur, Malaysia

as ultrafiltration have been widely used in fruit juice processing (Mohammad et al. 2012; Ilame et al. 2015). The effectiveness of ultrafiltration in separating anthocyanin and flavonols from black currant juice (Pap et al. 2012), phenolic compounds from pomegranate juice (Conidi et al. 2017), bioactive compounds from kiwifruit juice (Cassano et al. 2008), polyphenols from banana juice (Sagu et al. 2014), and phenolics from broccoli juice (Yilmaz and Bagci 2019) has been clearly demonstrated. Gulec et al. (2017) analysed membrane fouling during the ultrafiltration of apple juice. Although works on many fruit juices have been reported, there is no report on the separation of phytosterols from orange juice by ultrafiltration.

Orange juice contains bioactive compounds such as phytosterols (Piironen et al. 2003; Jiménez-Escrig et al. 2006; Balme and Gulacar 2012), sugars (Jesus et al. 2007), and protein (Okino Delgado and Fleuri 2016). The composition of orange juice is shown in Table 1. Orange juice contains a polydisperse distribution of particle sizes from pulp trashes to small particles less than 2 μm in diameter (Corredig et al. 2001; Stinco et al. 2012). In addition, the molecular weight of proteins in orange juice was 12 to 71 kDa (Sass-Kiss and Sass 2000). No literature is available on the performance of ultrafiltration processes for the separation of phytosterols from proteins in fruit juices. Our previous study was performed using three types of 10-kDa molecular weight cut-off (MWCO) ultrafiltration (UF) membranes made from regenerated cellulose (RC), polyethersulphone (PES), and fluoropolymer (FP). The 10-kDa regenerated cellulose membrane displayed the best rejection ratio of phytosterols (32%) from proteins in orange juice (Abd-Razak et al. 2019). Thus, process optimisation is important since the phytosterol yield was relatively low. It is hypothesised that the membrane with a larger MWCO can be used to transmit lower molecular weight compounds passing through the membrane.

This paper investigates the surface science of membrane fouling and cleaning processes and builds upon our previous study (Abd-Razak et al. 2019) which demonstrated the principle of using ultrafiltration to separate phytosterols from proteins in orange juice. This paper describes the isolation of phytosterols from orange juice for nutraceutical fabrication via an ultrafiltration process using regenerated cellulose membranes at different MWCO values. This study elucidates the mechanisms of fouling and flux loss, whilst optimizing the ultrafiltration process to fractionate the targeted sterol compounds. The performance of the separation is evaluated in terms of flux, rejection, membrane resistance, and cleaning efficiency. Contact angle measurement, atomic force microscopy (AFM), Fourier transform infrared (FTIR) spectroscopy, and scanning electron microscopy (SEM) were carried out to investigate the membrane surface modification occurring as a result of ultrafiltration.

Materials and Methods

Materials

Chemicals and standards used in this work are listed in Table 2. All solvents and reagents were purchased from Merck (UK). Butylated hydroxytoluene and stigmasterol sourced from Sigma-Aldrich (UK) were used as characterisation standards. The protein assay kit was acquired from Bio-Rad (UK). Cleaning of membranes was carried out using 0.5 wt%. P3-Ultrasil 11 (Henkel Ecolab, USA) which contains sodium hydroxide, tetrasodium salt of EDTA, anionic surfactant, and non-ionic surfactant (Weis et al. 2005).

Membranes

Three flat-sheet regenerated cellulose acetate (RCA) membranes with 10-kDa, 30-kDa, and 100-kDa MWCO values, were supplied by Alfa Laval (Denmark). RCA 10 kDa is a commercial membrane with Alfa Laval code RC70PP. RCA 30 and 100 kDa are prototype membranes. The characteristics of membranes are summarised in Table 3 (Alfa-Laval 2017). Membranes were cut to size with a membrane area of 336 cm^2 and placed in the membrane module. Prior to filtration, new membranes were conditioned by passing reverse osmosis (RO) water through the membrane at 60 °C and at TMP of 1 bar for 120 min. This conditioning technique was established to remove glycerol coating from the membrane surface applied by the manufacturer (Weis et al. 2003).

Pre-filtration of Orange Juice

Processed orange juice (not from concentrate) was sourced from Cobell (UK). At the factory, the processing begins with

Table 1 Composition of orange juice in term of phytosterols, protein, and sugar contents

Components	Amount	
	This study	Literature
Phytosterols	0.2–0.3 mg/ml	0.2–0.3 mg/ml (Piironen et al. 2003; Jiménez-Escrig et al. 2006)
Protein	0.8–1.0 mg/ml	0.7–0.9 mg/ml (Cobell 2016)
Sugar	10–11°Brix	≥ 10°Brix (Cobell 2016)

Table 2 Chemicals and standards used

Chemical	Function	Analysis
Chloroform	Solvent	Total phytosterol content
Acetic anhydride	Reagent	Total phytosterol content
Sulphuric acid	Reagent	Total phytosterol content
Stigmasterol	Standard	Total phytosterol content
Methanol	Solvent	Antioxidant assay
1,1-Diphenyl-1-picrylhydrazyl (DPPH)	Reagent	Antioxidant assay
Butylated hydroxytoluene (BHT)	Standard	Antioxidant assay
Protein assay kit (dye reagent)	Reagent	Protein assay
Bovine serum albumin (BSA)	Standard	Protein assay

the washing process, and then, the fruit was placed in an extractor to separate the juice from the pulp and skin. It was then centrifuged to push the juice out and finally pasteurised to reduce microbiological loading whilst maintaining as much of the colour, flavour, and aroma of the fruit (Cobell 2016). Processed orange juice was received in a bulk (100 L/ batch) and then stored in a cold room at 4 °C up to 2 months. The juice was first pre-filtered through a stainless steel 25-μm cartridge filter (Memtech, UK) that was attached to an Amicon (Danvers, USA) pressurised feed vessel, to remove pulp prior to ultrafiltration. The pre-filtration was carried out at 1.5 bar at room temperature.

Ultrafiltration Experimental Setup

Three RCA membranes of each MWCO (10 kDa, 30 kDa, and 100 kDa) were used in the experiments. Each membrane sample was run at three different cycles. The standard deviation was calculated based on three membrane samples for each MWCO. The ultrafiltration experiments were carried out by using a cross-flow membrane filtration system LabStak M10 containing four polymeric flat sheet membranes in series, manufactured by DSS (now Alfa Laval) (Denmark) with a total filtration area of 336 cm². The ultrafiltration was performed using 3 L orange juice for each run. Additional details concerning the ultrafiltration apparatus and the schematic

design of the system can be found in Abd-Razak et al. (2019). The ultrafiltration fouling and cleaning cycle consists of membrane conditioning, pure water flux (PWF), filtration, rinsing, and cleaning steps (Abd-Razak et al. 2019). Permeate flux was measured during the ultrafiltration of orange juice. Pure water flux (PWF) values were measured for membranes using RO water under these conditions: (i) before fouling, (ii) after fouling, and (iii) after cleaning at three different cycles. The cross-flow filtration cycle protocol is including PWF before fouling (10 min), filtration using orange juice (60 min), rinsing (5 min), PWF after fouling (10 min), cleaning (10 min), rinsing (5 min), and PWF after cleaning (10 min). The temperature of the feedstock was maintained at 20 ± 1 °C. A TMP value of 1.0 bar was used and the cross-flow velocity (CFV) was in the range 1.4–1.5 m s^{-1}. The PWF of the membrane was determined using RO water at three different times; before filtration, after first rinsing, and after cleaning. The filtration time was limited to 60 min, as this is sufficient to obtain a pseudo steady-state permeate flux.

Evaluation of Membrane Performance and Fouling Process

The membrane performance was evaluated in terms of permeate flux, resistances, rejection ratio, and fouling index (Mulder 1996). The permeate flux is defined as the volumetric flow

Table 3 Characteristics of the RCA membranes (from Alfa Laval (Alfa-Laval 2017))

Membrane	RCA 10	RCA 30	RCA 100
Manufacturer	Alfa Laval		
Material for selective layer	Regenerated cellulose acetate (RCA)		
Material for support layer	Polypropylene (PP)	Polyethylene terephthalate (PET)	
MWCO (kDa)	10	30	100
pH operating range	1–10		
pH cleaning	1–11.5		
Operating pressure (bar)	1–10		
Operating temperature (°C)	5–60		
Pure water permeance (L m^{-2} h^{-1} bar^{-1}) at 1.0 bar	100 ± 5	240 ± 5	210 ± 5

rate of the fluid through the membrane. The permeate flux through a membrane can be calculated using Eq. (1):

$$J = \frac{\Delta P}{\mu R tot} \tag{1}$$

where J is the flux through the membrane (L m^{-2} h^{-1}), ΔP (Pa) is the transmembrane pressure (TMP), μ is the dynamic viscosity (Pa s) and R_{tot} represents the total resistance (m^{-1}). The flux decline can be calculated using Eq. (2):

$$\text{Flux decline} = \frac{J0 - J\text{SS}}{J0} \tag{2}$$

where J_0 is the initial permeate flux and J_{ss} is the steady-state permeate flux. In pressure-driven processes such as ultrafiltration, fouling can be represented in the resistance in a series model as shown in Eqs. (3) and (4) (Jiraratananon and Chanachai 1996):

$$J = \frac{\Delta P}{\mu \left(Rm + Rf + Rcp \right)} \tag{3}$$

$$Rf = Rir + Rr \tag{4}$$

where R_m is the resistance of conditioned virgin membrane, R_f is the total fouling resistance, R_{ir} is the irreversible fouling resistance, R_r is the reversible fouling resistance, and R_{cp} is the resistance due to concentration polarisation. R_m is determined by measuring the flux of RO water through the conditioned membrane. Irreversible fouling is defined as any foulant not being removed by rinsing. Reversible fouling is defined as any foulant is removed from the membrane pores and surfaces by rinsing.

The cleaning efficiency was determined by comparing the pure water permeability before and after cleaning (Conidi et al. 2017). Selectivity is the degree to which one component preferentially permeates the membrane and thus determines the degree of enrichment achieved. Selectivity is expressed as the rejection ratio (R) and can be calculated by using Eq. (5); where C_p is the solute concentration in the permeate and C_r is the solute concentration in the retentate (Mulder 1996).

$$R = \left(1 - \frac{Cp}{Cr} \right) \tag{5}$$

Hermia divided fouling into four mechanisms namely cake filtration, standard blocking, intermediate pore blocking, and complete pore blocking (Hermia 1982). An analytical model was produced by Field et. al. (Field et al. 1995) based on Hermia's pore-blocking laws:

$$-\frac{dJ}{dt} J^{n-2} = k \left(J - J^* \right) \tag{6}$$

where J is flux, J^* is limiting flux, t is time, and n and k are constants specific to the type of fouling. The different fouling laws concerned are cake filtration, intermediate blocking, and complete blocking where n values are 0, 1, and 2 respectively. This model suggests that the fouling mechanism takes place sequentially (not simultaneously) from intermediate pore blocking and then cake filtration (Lewis et al. 2017). According to Eq. (6), a function of flux can be described as:

$$f(J) = -\frac{dJ}{dt} J^{n-2} \tag{7}$$

where a linear relationship between $f(J)$ and J is observed (Field et al. 1995). Experimental flux data was analysed to evaluate the type of membrane fouling using a MATLAB script (Lewis et al. 2017). Flux data shows $f(J)$ as described by Eq. (7) where $n = 0$ for cake filtration and $n = 1$ for intermediate pore blocking. The calculated data from MATLAB was re-plotted in Excel to determine the correlation coefficient of the graph using a linear regression type. The Hermia model is more reasonable when results fit a straight line (Nguyen et al. 2015).

Characterisation Techniques

Feed, permeate, and retentate samples from ultrafiltration experiments were collected and kept frozen at -18 °C until analysed. After thawing, the samples were vortex-mixed for 3 min at room temperature to homogenise the samples. Samples were analysed for total phytosterols, proteins, sugars, and antioxidant activity. All measurements were done in triplicate and the results were averaged. These analyses were used in the calculation of the rejection ratio.

The total phytosterol content was determined calorimetrically using a modified Liebermann-Buchard (LB)-based method (Mbaebie et al. 2012; Sathishkumar and Baskar 2014; Tolve et al. 2018). Formation of a green colour indicated the presence of phytosterols at absorbance 420 nm using an ultraviolet-visible (UV-Vis) spectrophotometer (Cary 100, Agilent, USA). Standard solutions of stigmasterol were used for the calibration. Protein concentration was quantified by the Bradford method (Cassano et al. 2008; Kruger 1994). The assay is based on the binding of the acidic dye solution Coomassie Brilliant Blue G-250 to protein at absorbance 595 nm (Bradford 1976). Bovine serum albumin (BSA) was used as a standard solution.

The sugar content expressed as °Brix was determined using a digital hand-held refractometer (Reichert, New York, USA).

The refractometer measures the refractive index which indicates the degree to which the light changes direction when it passes through the fruit juice. The antioxidant activity was measured by detecting the scavenging of 1, 1-diphenyl-2-picrylhydrazyl (DPPH) radical (Iqbal et al. 2015) at absorbance 517 nm using an ultraviolet-visible (UV-Vis) spectrophotometer (Cary 100, Agilent, USA). Butylated hydroxytoulene was prepared in methanol as reference.

Membranes Characterisation

Contact Angle

Contact angle measurements were conducted to evaluate the hydrophobicity of the membranes via sessile drop technique using DataPhysics Optical Contact Angle System OCA 25 (Filderstadt, Germany) equipped with image processing software DataPhysics Instruments SCA 22. Membranes were dried at 20 °C for 30 min. A deionised water droplet of 5 μL at the end of a syringe needle was deposited onto the membrane surface. The contact angle values were determined as the averaged values during measurement periods of 300–500 frames in 10–15 s (Baek et al. 2012). The procedure was repeated five times at different points on the same membrane sample. All measurements were done in triplicates.

Atomic Force Microscopy

The surface roughness values of the membrane surfaces were determined by atomic force microscopy (AFM). The flexible cantilever and the AFM tip gently touch the surface and record the small force between the tip and the surface (De Oliveira et al. 2012). This measurement was performed using a Multimode AFM (Veeco Metrology, USA) with a Nanoscope Analysis 1.7 software. The cantilever was used in contact mode with silicon soft tapping mode tips (Tap150AI-G, Budget Sensors, Bulgaria). Images were scanned at 1 μm × 1 μm scan size at a rate of 1 Hz for conditioned membranes, fouled membranes, and cleaned membranes. Samples were analysed in three replicates for the AFM analysis.

Fourier Transform Infrared Spectroscopy

Attenuated total reflection-Fourier transform infrared (ATR-FTIR) (Frontier FTIR, PIKE Technologies Inc., USA) was used to examine the foulant on the membrane surfaces due to fouling. Three fouled membrane samples were prepared for each molecular weight cut-off. The membrane samples were dried at room temperature for 24 h prior to analysis (Pihlajamäki et al. 1998). The FTIR apparatus was used to record the IR-spectra at the mid infrared (MID) region. The

scan speed was 0.2 cm^{-1} and a spectral resolution of 4 cm^{-1} using a KBr beam splitter was used in this study.

Scanning Electron Microscope and Energy-Dispersive X-Ray

Air and vacuum-dried membranes were mounted on aluminium stubs with conductive paste and gold sputter coated on a sputter coater model E150B (Edwards, UK) under argon gas.

Then, the samples were viewed with a JEOL SEM model JSM 6480LV (Japan). The elemental composition of a material on the membrane surface was examined by energy-dispersive X-ray (EDX) attached to the SEM. High-sensitivity Oxford INCA X-Act SDD X-ray detector (Oxford Instruments, UK) was used for EDX analysis.

Gel Permeation Chromatography

Gel permeation chromatography (GPC) analysis was carried out to study the polymer composition of three different RCA membranes by determining the distribution of molecular mass of polymer repeating unit in the membranes. Conditioned membranes were dissolved in tetrahydrofuran (THF) to give a concentration of 2 mg ml^{-1}. The solutions were left overnight at 4 °C prior to the GPC analysis. The molecular weight (MW) of the samples were determined using a 1260 GPC/SEC system (Agilent Technologies, USA) attached to a 2× PLgel 5-μm MIXED-D (7.5 × 300 mm) column and refractive index detector. The data was generated using Agilent GPC/SEC software. THF was used as the mobile phase.

Matrix-Assisted Laser Desorption Ionisation

Bruker AutoFlex matrix-assisted laser desorption ionisation (MALDI) mass spectrometer was used for polymer analysis of three different RCA membranes. Conditioned membranes were dissolved in two different solvents (THF and dichloromethane). Solvents were prepared at a concentration of 1 mg/ml. THF was used as the eluent. Dithranol and dihydroxybenzoic acid were used as the matrix.

Results and Discussion

Flux Analysis

Permeate Flux

At the beginning of the experiment, a 5-kDa membrane was also tested. The membrane showed a low permeate flux (10 L m^{-2}) at a TMP of 1.0 bar. Therefore, the experiment was continued with a 10-kDa membrane. Figure 1 presents the time course of permeate flux for orange juice ultrafiltration using RCA membranes for the three different MWCO values

tested. It can be seen in Fig. 1 that the trend for permeate flux for UF by using all membranes was similar. The initial permeate flux decreased gradually with filtration time until it reached a steady-state value. At the beginning of the ultrafiltration, the permeate fluxes for RCA 10, RCA 30, and RCA 100 were 29 L m^{-2} h^{-1}, 39 L m^{-2} h^{-1}, and 42 L m^{-2} h^{-1} respectively. After approximately 2 min, permeate fluxes continued to decline gradually until the filtration was stopped at 60 min. All membranes displayed steady-state permeate flux at ca. 22 L m^{-2} h^{-1}. In the previous studies (Abd-Razak et al. 2019), the steady-state flux of ca. 22 L m^{-2} h^{-1} was obtained at a TMP of 1.0 bar using RCA 10 kDa membrane. A steady-state flux value of 17 L m^{-2} h^{-1} was obtained for the PES 10-kDa membrane. The fluoropolymer 10-kDa membrane reached a steady-state value at 14 L m^{-2} h^{-1}. It can be concluded that the highest steady-state flux was achieved using the RCA membrane. Higher flux resulted in less total resistances. Thus, filtration using the RCA membrane has been selected in this study. The permeate flux of RCA 10, RCA 30, and RCA 100 dropped to 22 L m^{-2} h^{-1}, indicating a flux decline of 24%, 44%, and 48% respectively. It is notable that the steady-state permeate flux value is the same for all three membranes tested, irrespective of the MWCO value. The decrease of permeate flux can be explained by the effect of fouling (Conidi et al. 2017).

Pure Water Flux

Figure 2 shows the PWF of the membranes tested at TMP of 1.0 bar, CFV of 1.5 m s^{-1}, and at 20 °C. In general, the RCA 10 kDa and RCA 100 kDa membranes showed lower pure water fluxes than the RCA 30 kDa membrane. The PWF decreased in the following order, RCA30 > RCA100 > RCA10 which was not correlated with the MWCO of the membranes. The RCA 30 membrane with the intermediate MWCO (30 kDa) gave the highest water flux of 226–289 L m^{-2} h^{-1}. Meanwhile, RCA 100 with the highest MWCO (100 kDa) gave the PWF of 170–219 L m^{-2} h^{-1} and the RCA 10 membrane displayed the lowest water flux of 77–132 L m^{-2} h^{-1}. This may suggest that PWF was a poor indicator of permeate flux in this system as the higher MWCO membrane showed lower fluxes. The PWF (PWF2) was reduced after fouling for all membranes in all cycles. These results indicate that the ultrafiltration process was affected by the membrane fouling. Thus, a good cleaning method is required to regenerate the membrane.

The commercial cleaning formulation, Ultrasil 11 was used—this product finds wide application for membrane cleaning in laboratory situations (Wu and Bird 2007). Figure 2 demonstrates that the pure water permeate flux of the membrane after cleaning was higher than that seen after fouling (e.g. PWF 3 III > PWF 2 III). It is possible that surface modification is occurring due to the adsorption of the Ultrasil 11 surfactant to the membrane surface (Weis et al. 2003). It can be concluded that the cleaning technique is effective in regenerating the membrane. However, the membranes behave differently for the first cycle of RCA 10 and RCA 30 filtration, during which the fluxes after cleaning were higher than those recorded for the membrane before fouling (e.g. PWF 3 I > PWF 1 I). Hydrophobicity, charge, and roughness all affect the filtration process, and it is usual for these factors to dominate species/pore size considerations when examining small pore UF membranes. The results presented in Fig. 2 also demonstrate that the PWF for all membranes did not vary following three fouling/ cleaning cycles.

The membranes were also compared in terms of cleaning efficiency. The cleaning efficiency was evaluated by comparing the pure water permeability values before fouling and after cleaning (Conidi et al. 2017). The pure water permeabilities were taken from each cycle, which were then averaged. Table 4 displays the cleaning efficiency measured for all membranes tested. All three membranes (RCA 10, RCA 30, and RCA 100) displayed high cleaning efficiencies of greater than 97%. From this observation, it can be concluded that the chemical cleaning method using 0.5 wt% Ultrasil 11 was effective in regenerating all of the membranes tested [39].

Fig. 1 Time course of permeate flux decline for RCA membranes tested. The largest error for this set of data is ± 1.2 L m^{-2} h^{-1}. Data are shown as averages of 3 replicates of each membrane; error bars represent the standard deviation
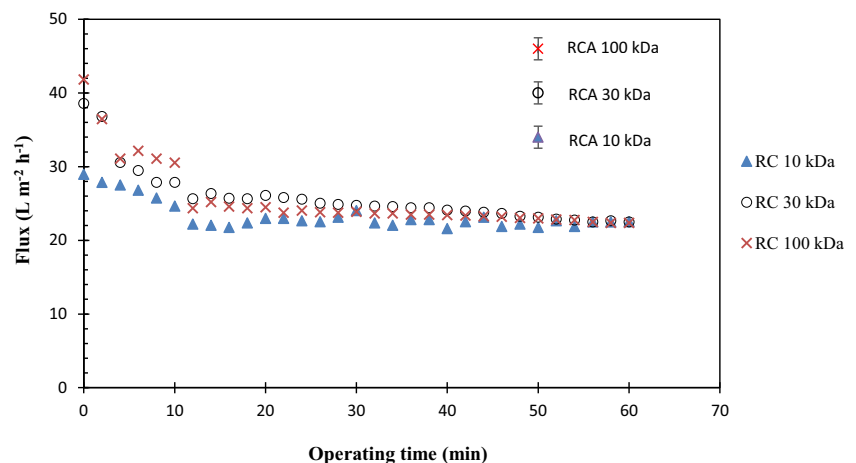
Fig. 2 Pure water fluxes of three membranes tested; RCA 10, RCA 30, and RCA 100 during three filtration cycles (1 h of fouling, 10 min of pure water flow, 10 min of cleaning) operated at TMP = 1 bar. Regions identified by Roman numerals represent the three filtration cycles. Average uncertainty of the pure water flux is ± 2 L m^{-2} h^{-1}. The error represents the standard deviation
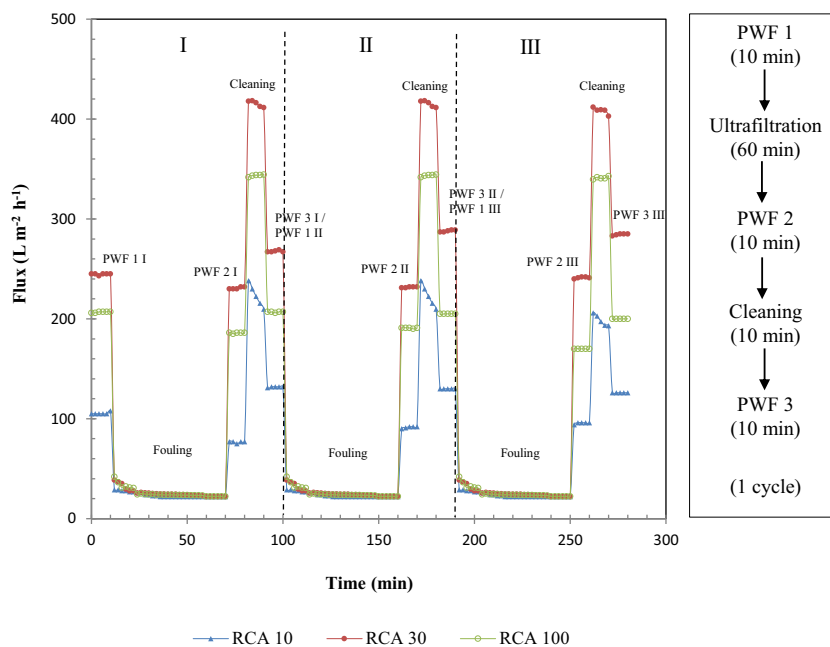
Resistances

Flux measurements were used to calculate the total resistances, including those due to the membrane, concentration polarisation, reversible fouling, and irreversible fouling (Eq. 2). The rejection of components at the membrane surface will lead to an increase in the viscosity of the retentate close to the membrane surface. However, the flux is primarily a function of the viscosity of the permeate through the pores. The viscosity of the feed is important in forming resistances such as by gelation and concentration polarisation (CP). A diagnostic test for CP was carried out whereby the feed pump was turned off and 60 s later turned on again. No jump in flux was seen, and accordingly, it is concluded that concentration polarisation is not an important fouling related resistance in this system.

Figure 3 shows the total resistances including membrane, reversible fouling, and irreversible fouling for the membranes were tested. The conditioned virgin membrane resistances before fouling for RCA 10, RCA 30, and RCA 100 were 3.0 × 10^{12} m^{-1}, 1.7 × 10^{12} m^{-1}, and 1.5 × 10^{12} m^{-1} respectively. After fouling, the total resistances increased to 4.7 × 10^{12} m^{-1}, 3.0 × 10^{12} m^{-1}, and 2.6 × 10^{12} m^{-1} respectively,

which were 1.6, 1.8, and 1.7 times more than those seen before fouling. These results indicate that the membranes became fouled during filtration. The RCA 10 membrane displayed the highest total membrane resistance, most probably due to the fact that this membrane had the lowest MWCO value of 10 kDa. This is also reflected in the lowest pure water flux for RCA 10 in Fig. 2. The increase in the total resistance recorded after fouling was mainly due to reversible rather than irreversible fouling (Fig. 3). Table 5 shows the percentages of total resistances including membrane resistance, reversible fouling, and irreversible fouling. The conditioned virgin membrane resistances for RCA 10, RCA 30, and RCA 100 were 64%, 55%, and 59% respectively. The 10-kDa RCA membrane showed total fouling resistances of 36%. The 30-kDa and 100-kDa membranes displayed a higher percentage of total fouling resistances of 45% and 41% respectively. Reversible fouling showed a higher percentage compared with irreversible fouling as shown in Table 5. Thus, reversible fouling was found to play an important role in the flux decline in this system. Hydrophilic membranes were subject to more reversible fouling than irreversible fouling, which is in agreement with the findings of Metsamuuronen in ultrafiltration of

Table 4 Cleaning efficiency for RCA 10, RCA 30, and RCA 100 membranes

Membrane	Cleaning efficiency (%)
RCA 10 kDa	98 ± 1
RCA 30 kDa	98 ± 1
RCA 100 kDa	97 ± 1

Table 5 Percentages of the breakdown of total resistances

|	RCA 10 kDa	RCA 30 kDa	RCA 100 kDa
Membrane resistance (%)	64	55	59
Reversible fouling (%)	30	25	23
Irreversible fouling (%)	6	20	18
Total Resistances (%)	100	100	100

proteins using regenerated cellulose membrane (Metsamuuronen 2003).

Rejection of Key Compounds

Samples from the feed, retentate, and permeate streams were collected and characterised for total phytosterols, protein, sugar contents, and antioxidant activity. The separation efficiency and the effect of membrane fouling were characterised by measuring the rejection of key compounds such as phytosterols, protein, sugar, and antioxidant activity (Fig. 4). A desirable separation outcome is that a membrane shows a high rejection to protein and a low rejection to sterols. As reported previously (Abd-Razak et al. 2019) the 10-kDa RCA membrane displayed good separation efficiency with $32 \pm 4\%$ rejection of phytosterols. The 30-kDa and 100-kDa membranes displayed a higher rejection of phytosterols of $74 \pm 6\%$ and $58 \pm 4\%$ respectively. Protein was highly rejected ($96 \pm 1\%$ rejection) by the 10-kDa membrane. The 30-kDa and 100-kDa membranes gave lower rejection of protein of $69 \pm 3\%$ and $67 \pm 2\%$, respectively. It is possible that the larger pore membranes enabled protein-based foulants to enter the structure more deeply, and whilst this led to a lower rejection of proteins, it also led to a higher rejection of sterols due to species interaction inside the pore. It is postulated that the molecules are trapped inside the pore due to the steric effect (Han et al. 2008). The steric effect forms a diffusive barrier and creates an interaction between the pore walls and the molecules; which leading to pore blocking. The 10-kDa membrane was likely to be fouled with a cake of proteins, which enabled sterols to pass into the permeate. It can be noted that most proteins were rejected by the 10-kDa MWCO membrane, since the molecular weight of proteins in orange juice was 12 to 71 kDa (Sass-Kiss and Sass 2000). The higher molecular weight compounds were rejected by the smaller pore size membrane and this increased the fouling layer (Evans et al. 2008). This
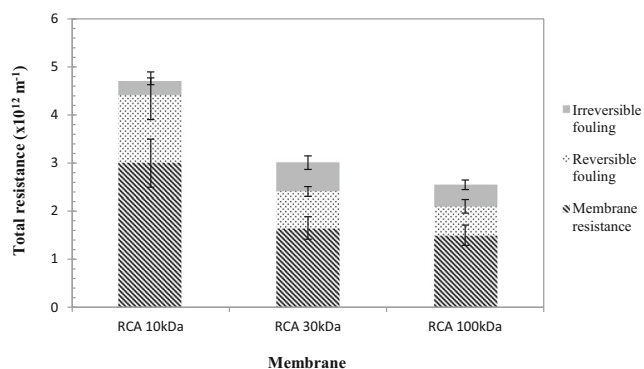
Fig. 3 Breakdown of total resistances during the ultrafiltration of phytosterols from orange juice using RCA 10, RCA 30, and RCA 100 membranes. Total resistances were divided into membrane resistance, irreversible fouling, and reversible fouling. Data are shown as averages of 3 replicates of each membrane; error bars represent the standard deviation
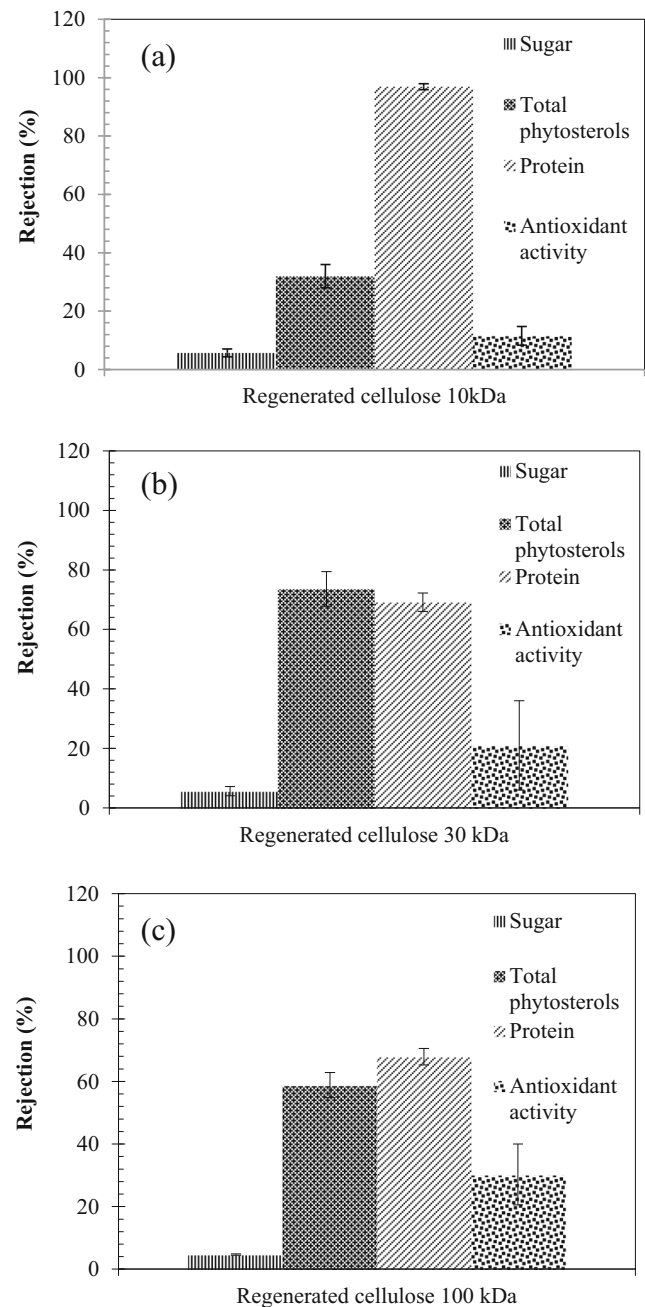
Fig. 4 Rejection of compounds by RCA membranes in term of total phytosterols content, protein, sugar, and antioxidant activity at 10-kDa (**a**), 30-kDa (**b**), and 100-kDa (**c**) membranes. Data are shown as averages of 3 replicates of each membrane; error bars represent the standard deviation

may suggest that the membrane was fouled by protein-based compounds that alter the selectivity of the membrane. This is supported by the modification of membrane hydrophobicity (Table 7) and surface roughness (Table 8) and also in agreement with the FTIR data (Fig. 6).

All membranes showed lower rejection of sugar (4% to 6%) in comparison to phytosterols and proteins. For antioxidant activity, the rejection was in the range 12 to 30%

inhibition. No correlation was observed between antioxidant activity and phytosterol content. It is possible that the antioxidant activity detected can be attributed to other chemical compounds present in orange juice, such as phenolic compounds (Stinco et al. 2012). According to these results, the RCA 10 kDa displayed the best separation with the highest transmission of phytosterols (32%) and the highest rejection (97%) of proteins from orange juice. Thus, it can be concluded that the RCA 10-kDa membrane is the best membrane in rejecting the protein from the sterols stream in orange juice.
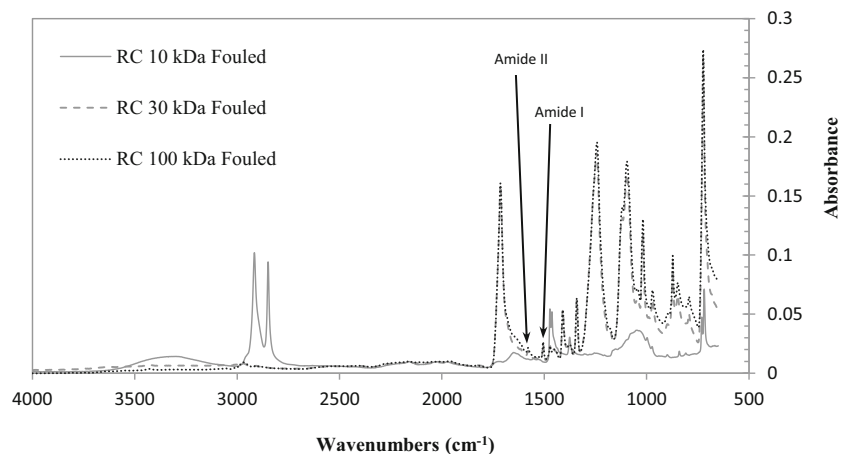
Hermia's blocking model was applied to all the filtration experiments. Hermia divided fouling into four mechanisms namely cake filtration, standard blocking, intermediate pore blocking, and complete pore blocking (Hermia 1982). According to Nguyen (Nguyen et al. 2015), the Hermia model is more reasonable when results fit a straight line. The fouling mechanism change at a flux transition point, J_T (Lewis et al. 2017; Iritani and Katagiri 2016). It should be noted that the flux in Fig. 5 is plotted on the x-axis with the filtration time moving in the direction from right to left. Figure 5 a and b show Hermia's blocking model applied to the RCA 10-kDa membrane. A linear line was seen from the beginning of the flux curve until the end of the filtration. A linear regression was applied in determining the correlation coefficient of the graph. The linear fit was limited to the linear region as shown in Fig. 5. The linear region for RCA 10 kDa was between 22 and 25 L m^{-2} h^{-1}. The correlation coefficient for RCA 10 kDa at $n = 0$ and $n = 1$ were 0.9795 and 0.9796 respectively (Fig. 5 a and b). Neither model showed a close fit to flux decline curves for the RCA 10-kDa membranes tested. However, it is postulated that the 10-kDa membrane was fouled with a cake of proteins, as proteins were highly rejected by the 10-kDa membrane as shown in Fig. 4.

The linear region for RCA 30 kDa was between 25 and 30 L m^{-2} h^{-1}. The correlation coefficient for RCA 30 kDa at $n = 0$ and $n = 1$ were 0.966 and 0.9891 respectively (Fig. 5 c and d). The linear region for RCA 100 kDa was between 24 and 30 L m^{-2} h^{-1}. The correlation coefficient for RCA

100 kDa at $n = 0$ and $n = 1$ were 0.9431 and 0.9756 respectively (Fig. 5 e and f). It can be seen in Fig. 5 c to f that Hermia's model indicates that the curve of $f(J)$ versus flux, J was more linear for $n = 1$ compared with $n = 0$, for RCA 30-kDa and RCA 100-kDa membranes, confirming that intermediate pore blocking was the dominant mechanism in both systems, particularly at high fluxes (i.e., initially during the filtration process). It could be that larger pore membranes enabled protein-based foulants to enter the structure more deeply. Transition points were observed for RCA 30-kDa and RCA 100-kDa membranes at $J = 25$ L m^{-2} h^{-1} and $J = 24$ L m^{-2} h^{-1} respectively. This suggests that a transition from intermediate pore blocking to cake fouling has occurred in both RCA 30-kDa and RCA 100-kDa membranes. In the intermediate blocking mechanism, some arriving particles are attached to the particles that are already deposited on the membrane surface. The cake filtration described the growth of particles on top of the membrane surface due to the accumulation and agglomeration of particles (Iritani and Katagiri 2016). Hermia's blocking model demonstrates the difference in the fouling mechanism for all three membranes based on flux data. This may suggest that the membranes fouled by protein-based compounds change their selectivity. Fouled membranes also become rougher (Table 8) and marginally more hydrophilic (Table 7).

Table 6 presents a mass balance for the ultrafiltration of total phytosterols and protein using three different RCA membranes. The initial volume of the orange juice for the ultrafiltration was 3000 ml. The total phytosterols present in the feed solution were 780 ± 30 mg. The yields of total phytosterols in the permeate streams for RCA 10, 30, and 100 kDa were 135 mg, 34 mg, and 65 mg respectively. It can be seen in Table 6 that the mass concentration ratio of sterol to protein was reduced from 0.27 in the feed to 0.16 in the permeate for the ultrafiltration using RCA 30 kDa. The mass concentration ratio of sterol to protein changed from 0.27 in the feed to 0.31 in the permeate for the RCA 100-kDa membrane. The permeate from the RCA 10-kDa membrane showed the highest ratio

Fig. 6 Infrared spectra of protein foulants (which are represented by amide I and amide II) deposited on the different membranes tested

Fig. 5 Hermia's blocking model applied to the data obtained from the ultrafiltration of orange juice using different MWCO membranes: RCA 10 kDa (**a**) and (**b**), RCA 30 kDa (**c**) and (**d**), and RCA 100 kDa (**e**) and (**f**). Data shows $f(J)$ as described by Eq. (7) where $n = 0$ for (**a**), (**c**), (**e**) and $n = 1$ for (**b**), (**d**), (**f**). The linear trendline is shown in grey lines. Red lines indicate the linear region
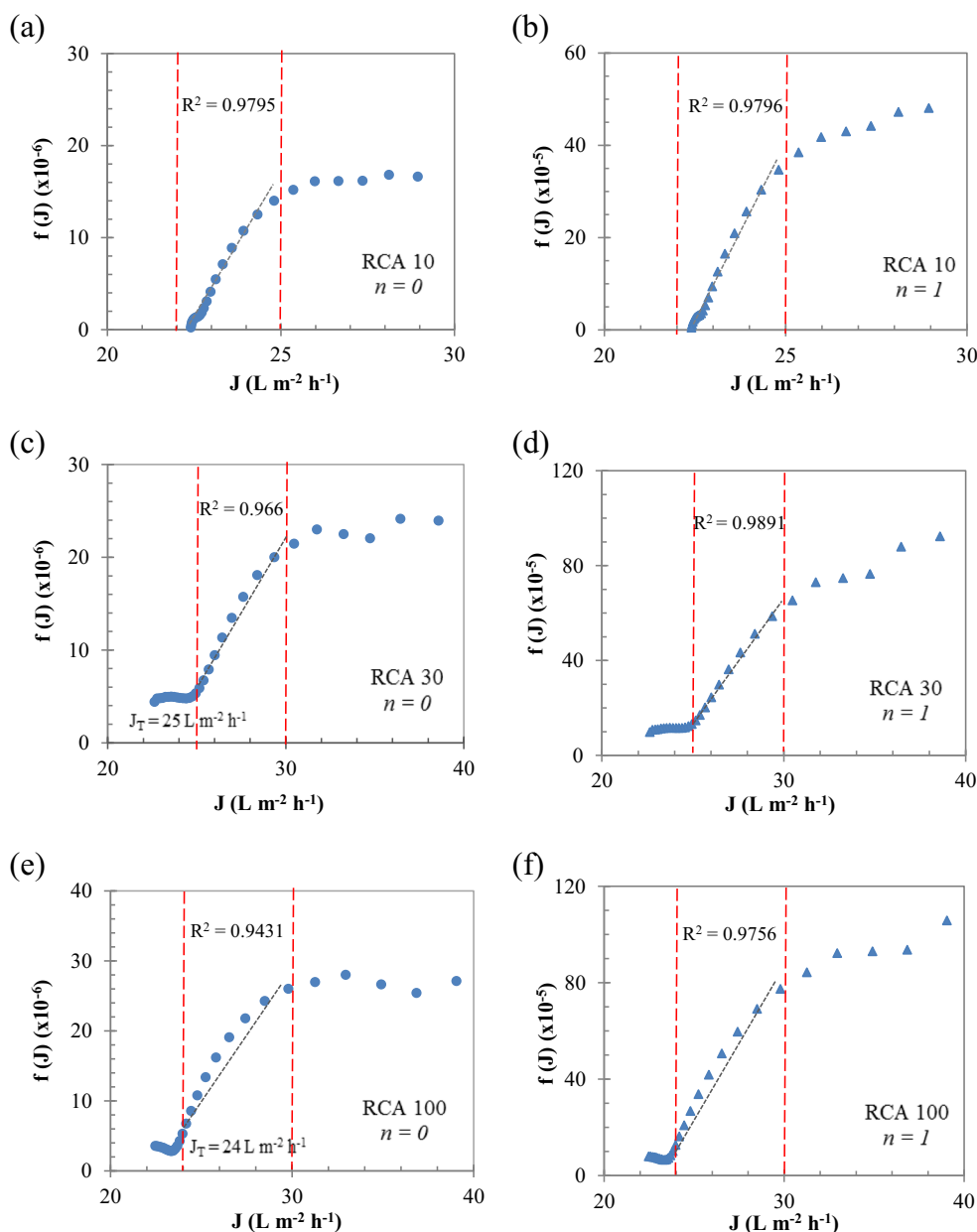
of sterols to protein than the feed. The ratio of the mass of phytosterols to protein for the RCA 10 membrane in the feed was 0.27 and in the permeate was 5.0. This result represented an increase in the ratio of sterol to protein of 18.5 when the permeate was compared with the feed. The 21% loss of phytosterols in the system for RCA 10 membrane, 50% loss for RCA 30, and 28% loss for RCA 100 membranes were most probably due to the fouling effect during the filtration (Cassano et al. 2008). The higher rejections seen in Table 6 for RCA 30 and RCA 100 membranes are linked to a greater loss of phytosterols into the foulants. This may suggest that the sterols were trapped by the fouling layer and not passed through the membrane, and also incorporated into the fouling.

In addition, protein in the feed solution was ca. 2850 ± 60 mg. The fraction of the original feed proteins still presents in the retentate after filtration for the RCA 10-, 30-, and 100-kDa membranes were 83%, 68%, and 71% respectively. The 16%, 24%, and 21% losses of the feed proteins for RCA 10, 30, and 100 membranes respectively were presumably due to the solute-membrane interaction and consequent adsorption of solute inside the membrane pores or on the membrane surface (Cassano et al. 2008). It can be noted that the highest recovery of phytosterols in the permeate was achieved by using RCA 10 membrane (43 ± 2 mg/L). Even though the sterol concentration in the permeate of RCA 10 kDa was lower than that in the feed, the permeate stream was relatively high in sterols and low in protein. This important result demonstrates that protein

Table 6 Mass balance for total phytosterols and protein by UF process of orange juice with different membranes: RCA 10, RCA 30 and RCA 100

	Feed	Retentate		Permeate		Total (%)
RCA 10						
Volume (ml)	3000	2150	72%	850	28%	100
Phytosterols (mg)	810	504	62%	135	17%	79
Protein (mg)	2910	2408	83%	26	1%	84
Mass concentration ratio (sterols to protein)	0.27			5.00		
RCA 30						
Volume (ml)	3000	2200	73%	800	27%	100
Phytosterols (mg)	773	359	46%	34	4%	50
Protein (mg)	2880	1958	68%	216	8%	76
Mass concentration ratio (sterols to protein)	0.27			0.16		
RCA 100						
Volume (ml)	3000	2240	75%	760	25%	100
Phytosterols (mg)	747	467	63%	65	9%	72
Protein (mg)	2790	1971	71%	213	8%	79
Mass concentration ratio (sterols to protein)	0.27			0.31		

can be removed from the sterols stream by using RCA 10 membrane. This theory is also supported by the rejection data.

Contact Angle Measurements

Membrane hydrophobicity was characterised by using contact angle data. All membranes tested were considered to be highly hydrophilic, as the contact angles measured were much less than 90° (Table 7). The contact angles of conditioned RCA 10, RCA 30, and RCA 100 membranes were $11 \pm 2°$, $13 \pm 2°$, and $18 \pm 2°$ respectively. The hydrophobicity of conditioned and fouled RCA membranes varied with MWCO such that RCA100 > RCA30 > RCA10. The hydrophobicity of conditioned RCA membranes was in agreement with findings by other researchers (Amy 2001; Nguyen et al. 2015; Mohammad et al. 2011). Membranes with more hydrophobic surface had higher fouling capacity than the ones with hydrophilic surface (Gulec et al. 2017). Table 7 also shows the contact angles of fouled membranes. All fouled membranes

displayed a contact angle of $10 \pm 2°$. It can be seen that the membranes became more hydrophilic after fouling. The contact angle measurements of fouled membranes showed the modification of membrane hydrophobicity due to protein-based foulants or other hydrophilic submicelles (Wu and Bird 2007; Argyle et al. 2015). This data supported the flux declining results, the membrane has been fouled during the filtration and it was modified after fouling. Cleaned membrane surfaces had contact angles between that of conditioned and fouled surfaces, implying that the membranes were not returned to their original state. However, within statistical error, no difference was detected between the contact angles of the conditioned and the cleaned membranes.

Surface Roughness by AFM

Atomic force microscopy (AFM) is an effective tool for the study of surface morphology and texture, including roughness, waviness, lay, and flaws (Kumar and Subba Rao 2012). In this study, the surface roughness of the RCA membranes has been investigated using AFM. The roughness of RCA membranes varied with MWCO such that RCA30 > RCA100 > RCA10 (Table 8). This result is in agreement with the flux analysis, FTIR spectra, and membrane surface analysis by SEM. The roughness value for the virgin conditioned RCA 10 membrane was similar to that reported in the literature (Evans et al. 2008). After fouling, all membranes displayed increased roughness values, indicating that relatively rough surface deposits were present (Jones et al. 2011). Membranes with rougher surfaces displayed a higher fouling capacity than those with smoother surfaces (Gulec et al. 2017). The foulant appears to be more highly entrapped by rougher surfaces. The surface roughness values were reduced

Table 7 Contact angles of water drops on RCA membranes

Membrane	Contact angle (°)			
	Conditioned		Fouled	Cleaned
RCA 10 kDa	11 ± 2	5[a], 10.2[b]	10 ± 2	8 ± 2
RCA 30 kDa	13 ± 2	12[c]	10 ± 2	12 ± 2
RCA 100 kDa	18 ± 2	18[a]	10 ± 2	15 ± 2

[a] From Amy (Amy 2001)

[b] From Nguyen (Nguyen et al. 2015)

[c] From Mohammad (Mohammad et al. 2011)

Table 8 Surface roughness values as measured by AFM

Membrane	Surface roughness (nm)		
	Conditioned	Fouled	Cleaned
RCA 10 kDa	3 ± 1	31 ± 2	10 ± 2
RCA 30 kDa	17 ± 1	42 ± 3	20 ± 2
RCA 100 kDa	10 ± 2	39 ± 2	15 ± 1

after cleaning but did not return to the initial roughness values. This may suggest that the surfaces have not been returned to a pristine condition.

Spectral Chemistry Determination Using FTIR

FTIR analyses allowed the identification of the functional groups present on polymeric membranes. The intensity of IR absorption bands was used qualitatively to identify changes in the composition of material present on membrane surfaces due to fouling and cleaning processes (Wu and Bird 2007). The FTIR spectra in the range of 4000–650 cm^{-1} were used to analyse the membrane surfaces at different conditions. Figure 6 displays the overlay results of FTIR spectra of fouled membranes for all RCA membranes. It was observed that all samples showed identical FTIR spectra with slightly shifted absorption bands. The intensity of RCA membrane deposits varied with MWCO such that RCA30 > RCA100 > RCA10. This also corresponds to the order of the increased surface roughness and pure water fluxes declining results. The higher intensity recorded demonstrated that more foulant was deposited on the membrane surface. Rougher membranes would potentially trap more foulants on the membrane surfaces (Evans et al. 2008). This demonstrated that more foulant was deposited on the RCA 30-kDa membrane. This result correlates well with the surface roughness and SEM analyses. The fouled membranes might be due to protein-based foulants or other hydrophilic submicelles (Wu and Bird 2007; Argyle et al. 2015). The area 1400–1800 cm^{-1} was studied for the presence of protein foulant on the membrane surface. The protein peaks can be identified in this area with two peaks called amide I peak at 1540 cm^{-1} and amide II peak near 1650 cm^{-1}. Amide I peak at 1540 cm^{-1} corresponds to C=O group stretching vibration. Meanwhile, amide II was due to the combination of –NH deformation and C–N stretching vibration (Metsamuuronen 2003). The amide peaks in the spectra of RCA 10 membrane are much lower than those presented in RCA 30 and RCA 100 membranes. C–H stretching vibration peaks at 2850 and 2900 cm^{-1} that were observed in RCA 10-kDa membrane are characteristic for polypropylene as it was used as the support layer.

Membrane Morphology by SEM

The morphology of the membranes was examined via scanning electron microscopy (SEM). SEM was used to visualise the differences of membranes before and after fouling and subsequent cleaning. Membrane surface images of RCA membranes tested are presented in Fig. 7. The surface structures of conditioned membranes in Fig. 7a, d, g were changed from a rather smooth surface to a rough surface on fouled membranes in Fig. 7b, e, h. Fouling is clearly seen on the fouled membrane surfaces which are in agreement with the contact angle, surface roughness, and flux results. The inspection on cleaned membrane surfaces in Fig. 7c, f, i shows that the cleaning method used is effective in removing the foulants. The presence of crystalline structures on fouled membrane surfaces was further evaluated by energy dispersive X-ray (EDX) analysis. The difference in surface morphology for the membrane is a function of the membrane formation process, which is related to the composition of the formulation. Although all membrane active layers were comprised of regenerated cellulose acetate, the RCA 30-kDa membrane contains one amphiphilic polymer. A particular pattern was formed on top of the membrane surface due to the self-assembly of this polymer. This created distinctive membrane surface properties (Guo 2018).

Studies on the membrane polymer composition have been carried out by using gel permeation chromatography (GPC) to determine polymer molecular weight distribution (Engel et al. 2012). Figure 8 shows the chromatogram of GPC analyses for the RCA 10-kDa membrane. All samples were dissolved in THF for 24 h in order to remove the coating layer of the polymeric membranes. It can be seen in Fig. 8 that there was a peak found indicating the presence of oligomers in RCA 10 as highlighted in the chromatogram. However, there was no peak detected for either the RCA 30 or the RCA 100 membranes. This may suggest that the polymer coatings were not dissolved in THF for either of the samples tested. Further investigation on the RCA 10 membrane was performed using matrix-assisted laser desorption ionisation (MALDI). Based on the chromatogram in Fig. 9, the mass region of ion peaks was observed with a peak-to-peak mass difference of ca. 300 $g\,mol^{-1}$. Thus, it can be concluded that RCA 10 contains polymer repeating units at a molar mass of ca. 300 $g\,mol^{-1}$. It can also be concluded that the polymer compositions of RCA 30 and 100 are different from those present for the RCA 10 membrane.

Elemental Analysis by EDX

The elemental examinations were carried out by energy-dispersive X-ray (EDX) analysis coupled with SEM, to investigate the elemental composition on the membrane surfaces. As displayed in Fig. 10, the RCA membrane consists of carbon (C) and oxygen (O) elements. These results are not surprising, given

Fig. 7 Scanning electron microscope (SEM) images of RCA membranes taken at × 10,000 or × 15,000 magnification RCA 10 kDa conditioned (**a**), RCA 10 kDa fouled (**b**), RCA 10 kDa cleaned (**c**), RCA 30 kDa conditioned (**d**), RCA 30 kDa fouled (**e**), RCA 30 kDa cleaned (**f**, RCA 100 kDa conditioned (**g**), RCA 100 kDa fouled (**h**), and RCA 100 kDa cleaned (**i**)
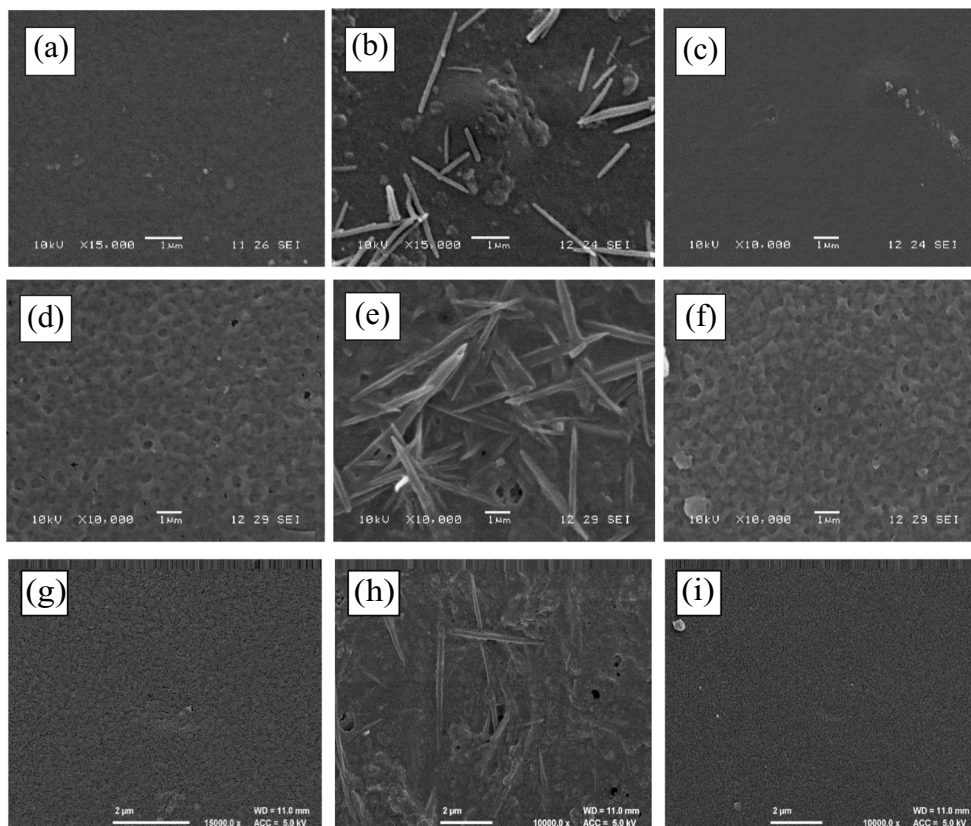

that the membranes were fabricated from cellulose (Li et al. 2014). It can be seen that the elements present in conditioned membranes were similar to the elements in cleaned membranes. This result correlates well with the FTIR and SEM analyses that suggest the membranes were regenerated effectively after the cleaning protocol was applied. Aluminium (Al) was found on certain membrane samples due to the aluminium stub used in the analysis. The EDX analyses for fouled membranes were focused on the crystalline structures. The fouled membranes were coated with gold prior to the EDX analysis at higher magnification. The crystalline structures could not be observed at low magnification. Therefore, gold (Au) was also observed on the fouled membranes.

The result in Fig. 10 confirms that potassium (K) elements exist on the membrane surfaces after fouling. According to the literature (Navarro et al. 2011; Schmutzer et al. 2016), potassium is present in orange juice in relatively high concentrations. Potassium in orange juice is commonly associated with citrate

Fig. 8 The chromatogram shows the GPC analysis of the RCA 10-kDa membrane. In the chromatogram, the refractive index (RI) detector signal is shown in light blue, the viscometer (VS) signal is shown in dark blue, and the light scattering (LS) signal is shown in yellow. A calibration curve is shown in a red line with blue dots. Blue columns indicate the beginning and end of the baseline. Peaks indicating the presence of oligomers in RCA 10 were highlighted in region 1 at ~ 17.5 min
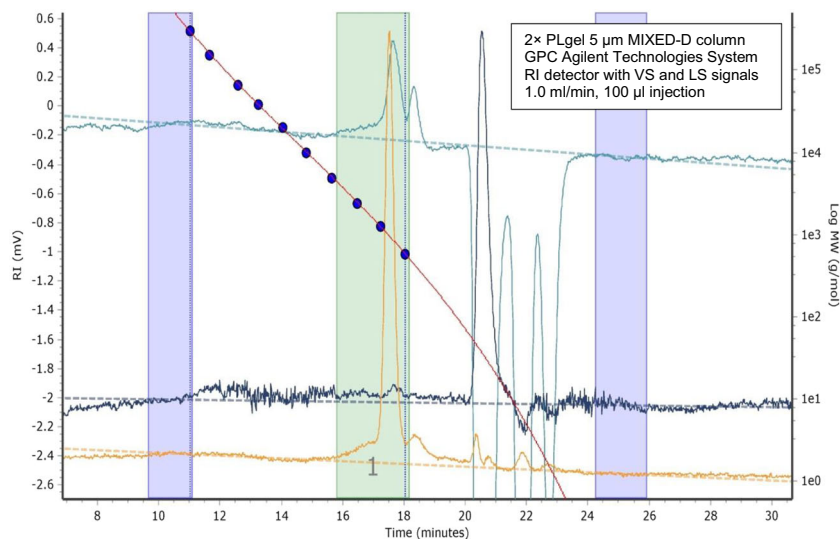
Fig. 9 MALDI mass spectra of RCA 10-kDa membrane analysed in positive ion mode by using dithranol and dihydroxybenzoic acid as matrices. The mass difference of ca. 300 $gmol^{-1}$ between neighbouring peaks is observed. The chromatogram shows polymer repeating units at a molar mass of ca. 300 $gmol^{-1}$ between m/z 400 and 1700
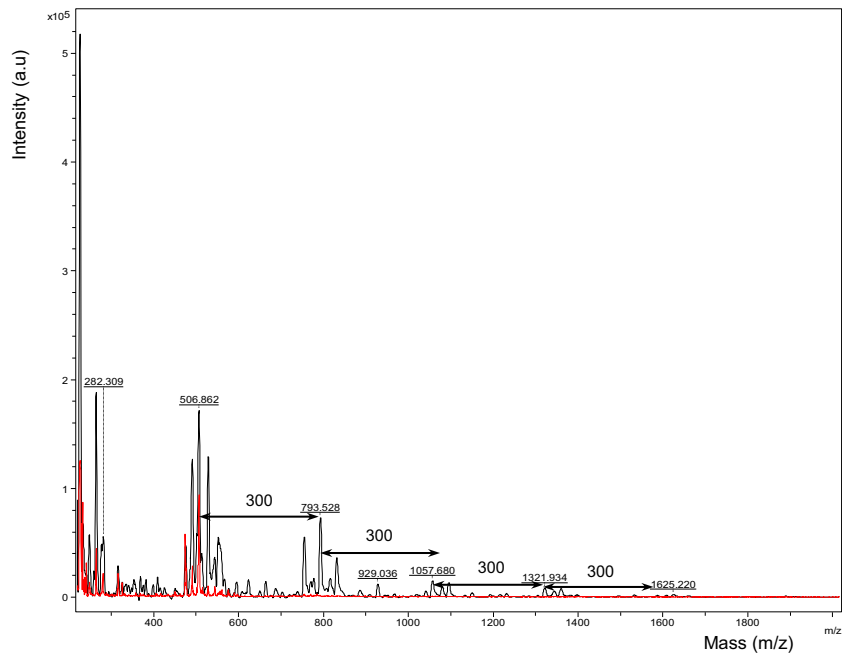
Fig. 10 SEM images with EDX analysis. SEM-EDX analysis was performed on RCA 10 kDa membrane surfaces at conditioned (**a**), fouled (**b**), and cleaned membranes (**c**). The EDX spectra are dominated by carbon (C) and oxygen (O) elements. Aluminium (Al) was found on the conditioned membrane (**a**). The fouled membrane (**b**) shows the presence of gold (Au) element
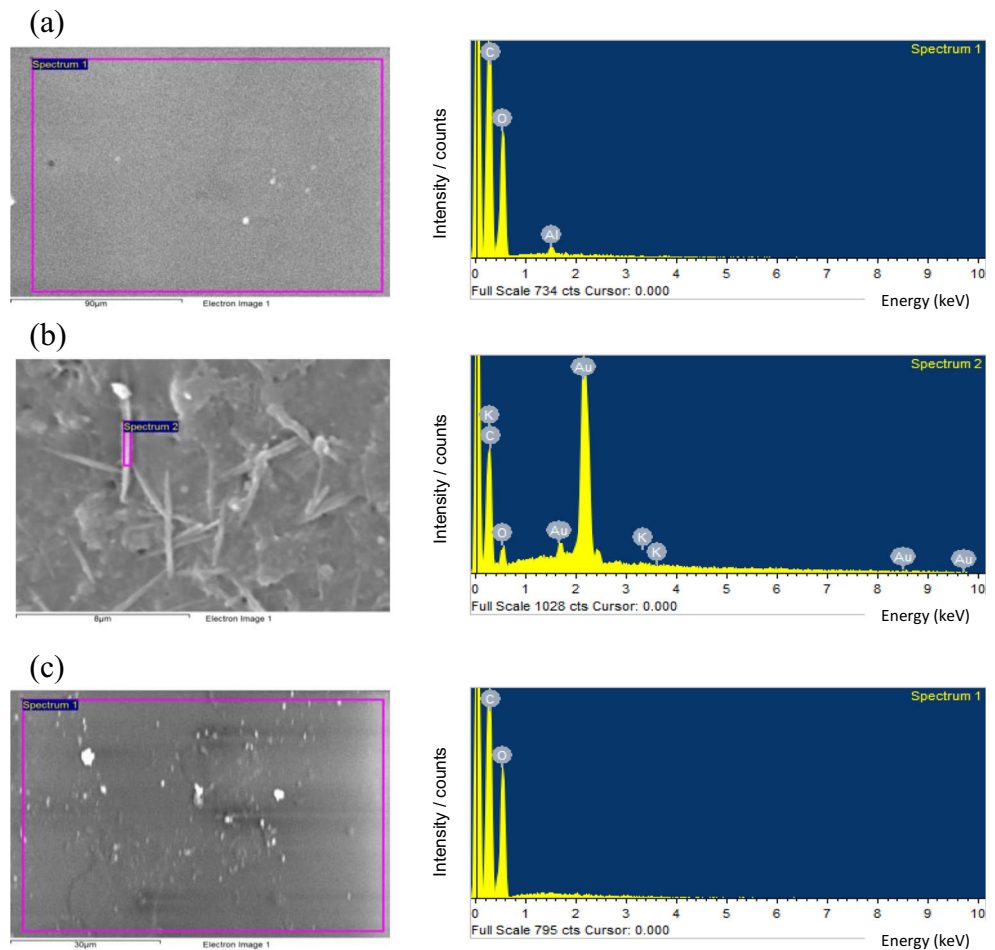
(Odvina 2006). Thus, it can be concluded that the crystalline structure on fouled membranes might be potassium salt which is potassium citrate. The potassium citrate was relatively hydrophilic which is in agreement with findings in contact angle and FTIR analyses that foulants might be due to hydrophilic submicelles (Argyle et al. 2015). In addition, the absorption band corresponding to potassium citrate was observed at 1650 cm^{-1} (stretching symmetric and asymmetric vibrations of COO groups) (Naidenko et al. 2012). However, this band was overlapping with the protein absorption band.

Conclusions

The effectiveness of regenerated cellulose acetate (RCA) based ultrafiltration membranes as a technology for isolating phytosterol from orange juice has been established. The isolation of phytosterols from orange juice has been studied by using RCA membranes with 10-kDa, 30-kDa, and 100-kDa MWCO. From the permeate flux analysis, product fluxes declined gradually to similar steady-state values. This indicates that the PWF was a poor indicator of product flux in this system, as fouling is key. Fouling layers change the membrane selectivity. All membranes exhibited steady-state permeate flux values of 22 L m^{-2} h^{-1}. Counter-intuitively, the smallest MWCO membrane tested (10-kDa RCA) gave the lowest rejection of phytosterols and hence the best performance. The RCA 10 membranes also gave the highest rejection of proteins, at 96%—a desirable result. However, fouling led to a reduction in the total amount of phytosterol presented in the system, leading to a reduction in the concentration of sterols in both the retentate and the permeate, when compared with the feed. The mass concentration ratio of sterol to protein changed from 0.27 in the feed to 5.0 in the permeate for the ultrafiltration using RCA 10 kDa.

Reversible fouling was found to play an important role in the flux decline. However, irreversible fouling for RCA 30 and RCA 100 membranes was higher than that seen for the RCA 10 membrane. It is postulated that proteins were trapped in the RCA 30 and RCA 100 membrane pores—this is supported by the Hermia flux decline analysis. It is possible that membranes with bigger pores trapped more protein-based foulants, or other hydrophilic compounds such as potassium citrate, than the small MWCO membrane. This leads to a change in membrane selectivity and an increased rejection of the smaller phytosterol molecules. Membranes after fouling and cleaning were found to have undergone surface modification including changes in hydrophobicity and roughness. The surface roughness and pure water flux decline of RCA membranes varied with MWCO, such that RCA 30 > RCA 100 > RCA 10. The RCA 10 membranes displayed the greatest hydrophilicity and the smoothest surface of the three membranes examined. Moreover, the fouling deposits presented on the RCA 10 membrane were the smoothest of the three fouled

membranes tested. These results confirmed that hydrophobicity and roughness were more important than molecular weight cut-off in determining the performance of UF membranes for the fractionation of sterols from proteins in orange juice filtration.

This result has important implications for the industrial application of this technology to process orange juice, and possibly other sterol-rich feeds. Based on this study, for a 15-m^2 RCA membrane with a 2-year shelf-life, the ultrafiltration costs using an M10 filtration system are estimated to be £23,500. Assuming that the total volume of orange juice filtered in 2 years is 21 tonnes, the profit is estimated to be £5000 after 2 years. Therefore, this paper presents some evidence which suggests that with this operating procedure, phytosterols and proteins can be separated from orange juice with the possibility of scaling up the process. Since the yield of phytosterol compounds separated by the 10-kDa RCA membrane was relatively low, there is the potential for process optimisation. Thus, the ultrafiltration will be carried out at different process temperatures. In future studies, the loss of sterols to the foulant layers will be addressed by increasing the total volume of feed filtered, whilst maintaining the membrane area at the same value, thereby increasing the total amount of sterol present in the system. Diafiltration may also be applied in concentrating the targeted compounds.

Compliance with Ethical Standards

Conflict of Interest   The authors declare that they have no conflicts of interest.

References

Abd-Razak, N. H., Chew, Y. M. J., & Bird, M. R. (2019). Membrane fouling during the fractionation of phytosterols isolated from orange juice. *Food and Bioproducts Processing, 113*, 10–21. https://doi.org/10.1016/j.fbp.2018.09.005.

Alfa-Laval. (2017). Alfa Laval - UF flat sheet membrane. https://www.alfalaval.co.uk/products/separation/membranes/flat-sheet-membranes/uf-flat-sheet/. Accessed 11 July 2019.

Amy, G. L. (2001). NOM rejection by, and fouling of, NF and UF Membranes. American Water Works Association.

Argyle, I. S., Pihlajamäki, A., & Bird, M. R. (2015). Black tea liquor ultrafiltration: effect of ethanol pre-treatment upon fouling and cleaning characteristics. *Food and Bioproducts Processing, 93*(Supplement C), 289–297. https://doi.org/10.1016/j.fbp.2014.10.010.

Baek, Y., Kang, J., Theato, P., & Yoon, J. (2012). Measuring hydrophilicity of RO membranes by contact angles via sessile drop and captive bubble method: a comparative study. *Desalination, 303*, 23–28. https://doi.org/10.1016/j.desal.2012.07.006.

Balme, S., & Gulacar, F. O. (2012). Rapid screening of phytosterols in orange juice by solid-phase microextraction on polyacrylate fibre derivatisation and gas chromatographic-mass spectrometric. *Food Chemistry, 132*(1), 613–618. https://doi.org/10.1016/j.foodchem.2011.10.097.

Bradford, M. M. (1976). A rapid and sensitive method for the quantitation of microgram quantities of protein utilizing the principle of protein-dye binding. *Analytical Biochemistry, 72*(1), 248–254. https://doi.org/10.1016/0003-2697(76)90527-3.

Cassano, A., Donato, L., Conidi, C., & Drioli, E. (2008). Recovery of bioactive compounds in kiwifruit juice by ultrafiltration. *Innovative Food Science & Emerging Technologies, 9*(4), 556–562. https://doi.org/10.1016/j.ifset.2008.03.004.

Cobell. (2016). *Orange juice not from concentrate (NFC)*. Exeter: Cobell.

Conidi, C., Cassano, A., Caiazzo, F., & Drioli, E. (2017). Separation and purification of phenolic compounds from pomegranate juice by ultrafiltration and nanofiltration membranes. *Journal of Food Engineering, 195*, 1–13. https://doi.org/10.1016/j.jfoodeng.2016.09.017.

Corredig, M., Kerr, W., & Wicker, L. (2001). Particle size distribution of orange juice cloud after addition of sensitized pectin. *Journal of Agricultural and Food Chemistry, 49*(5), 2523–2526.

De Oliveira, R. R. L., Albuquerque, D. A. C., Cruz, T. G. S., Yamaji, F. M., & Leite, F. L. (2012). *Measurement of the nanoscale roughness by atomic force microscopy: basic principles and applications, atomic force microscopy - imaging, measuring and manipulating surfaces at the atomic scale*. IntechOpen: Victor Bellitto.

Engel, P., Hein, L., & Spiess, A. C. (2012). Derivatization-free gel permeation chromatography elucidates enzymatic cellulose hydrolysis. *Biotechnology for Biofuels, 5*(1), 77–77. https://doi.org/10.1186/1754-6834-5-77.

Evans, P. J., Bird, M. R., Pihlajamäki, A., & Nyström, M. (2008). The influence of hydrophobicity, roughness and charge upon ultrafiltration membranes for black tea liquor clarification. *Journal of Membrane Science, 313*(1), 250–262. https://doi.org/10.1016/j.memsci.2008.01.010.

Field, R. W., Wu, D., Howell, J. A., & Gupta, B. B. (1995). Critical flux concept for microfiltration fouling. *Journal of Membrane Science, 100*(3), 259–272. https://doi.org/10.1016/0376-7388(94)00265-Z.

Gulec, H. A., Bagci, P. O., & Bagci, U. (2017). Clarification of apple juice using polymeric ultrafiltration membranes: a comparative evaluation of membrane fouling and juice quality. *Food and Bioprocess Technology, 10*(5), 875–885. https://doi.org/10.1007/s11947-017-1871-x.

Guo, H. (2018). *Personal Correspondance*. Denmark: Alfa Laval.

Han, J., Fu, J., & Schoch, R. B. (2008). Molecular sieving using nanofilters: past, present and future. *Lab on a Chip, 8*(1), 23–33. https://doi.org/10.1039/b714128a.

Hermia, J. (1982). Constant pressure blocking filtration laws–application to power law non-Newtonian fluids. *Trans Inst Chem Eng, 60*, 183–187.

Ilame, S. A., Singh, V., & S. (2015). Application of membrane separation in fruit and vegetable juice processing: a review. *Critical Reviews in Food Science and Nutrition, 55*(7), 964–987. https://doi.org/10.1080/10408398.2012.679979.

Iqbal, E., Salim, K. A., & Lim, L. B. L. (2015). Phytochemical screening, total phenolics and antioxidant activities of bark and leaf extracts of Goniothalamus velutinus (Airy Shaw) from Brunei Darussalam. *J King Saud Univ Sci, 27*(3), 224–232. https://doi.org/10.1016/j.jksus.2015.02.003.

Iritani, E., & Katagiri, N. (2016). Developments of blocking filtration model in membrane filtration. *KONA Powder and Particle Journal, 33*, 179–202. https://doi.org/10.14356/kona.2016024.

Jesus, D. F., Leite, M. F., Silva, L. F. M., Modesta, R. D., Matta, V. M., & Cabral, L. M. C. (2007). Orange (Citrus sinensis) juice concentration by reverse osmosis. *Journal of Food Engineering, 81*(2), 287–291. https://doi.org/10.1016/j.jfoodeng.2006.06.014.

Jiménez-Escrig, A., Santos-Hidalgo, A. B., & Saura-Calixto, F. (2006). Common sources and estimated intake of plant sterols in the Spanish diet. *Journal of Agricultural and Food Chemistry, 54*(9), 3462–3471. https://doi.org/10.1021/jf053188k.

Jiraratananon, R., & Chanachai, A. (1996). A study of fouling in the ultrafiltration of passion fruit juice. Journal of Membrane Science, 111(1), 39–48, doi:https://doi.org/10.1016/0376-7388(95)00270-7, 1.

Jones, S. A., Bird, M. R., & Pihlajamäki, A. (2011). An experimental investigation into the pre-treatment of synthetic membranes using sodium hydroxide solutions. *Journal of Food Engineering, 105*(1), 128–137. https://doi.org/10.1016/j.jfoodeng.2011.02.015.

Kongduang, D., Wungsintaweekul, J., & De-Eknamkul, W. (2012). Established GC-FID for simultaneous determination of diterpenes and phytosterols in Plaunoi (Croton stellatopilosus Ohba). *Songklanakarin Journal of Science and Technology, 34*, 623–628.

Kruger, N. J. (1994). The Bradford method for protein quantitation. *Methods in Molecular Biology, 32*, 9–15. https://doi.org/10.1385/0-89603-268-x:9.

Kumar, B., & Subba Rao, T. (2012). AFM studies on surface morphology, topography and texture of nanostructured zinc aluminum oxide thin films. *Digest Journal of Nanomaterials and Biostructures, 7*, 1881–1889.

Lewis, W. J. T., Mattsson, T., Chew, Y. M. J., & Bird, M. R. (2017). Investigation of cake fouling and pore blocking phenomena using fluid dynamic gauging and critical flux models. *Journal of Membrane Science, 533*, 38–47. https://doi.org/10.1016/j.memsci.2017.03.020.

Li, R., Liu, L., & Yang, F. (2014). Removal of aqueous Hg(II) and Cr(VI) using phytic acid doped polyaniline/cellulose acetate composite membrane. *Journal of Hazardous Materials, 280*, 20–30. https://doi.org/10.1016/j.jhazmat.2014.07.052.

Marangoni, F., & Poli, A. (2010). Phytosterols and cardiovascular health. *Pharmacological Research, 61*(3), 193–199. https://doi.org/10.1016/j.phrs.2010.01.001.

Market-Insights-Reports. (2019). Global phytosterols market insights, forecast to 2025. https://www.marketinsightsreports.com/reports/02011075734/global-phytosterols-market-insights-forecast-to-2025?source=nevadagreentimes&Mode=19. Accessed 16 April 2019.

Mbaebie, B. O., Edeoga, H. O., & Afolayan, A. J. (2012). Phytochemical analysis and antioxidants activities of aqueous stem bark extract of Schotia latifolia Jacq. *Asian Pacific Journal of Tropical Biomedicine, 2*(2), 118–124. https://doi.org/10.1016/S2221-1691(11)60204-9.

McDonald, J. G., Smith, D. D., Stiles, A. R., & Russell, D. W. (2012). A comprehensive method for extraction and quantitative analysis of sterols and secosteroids from human plasma. *Journal of Lipid Research, 53*(7), 1399–1409. https://doi.org/10.1194/jlr.D022285.

Metsamuuronen, S. (2003). *Critical flux and fouling in ultrafiltration of proteins*. Lappeenrannan: Lappeenrannan teknillinen yliopisto.

Mohammad, A., Hilal, N., Ying Pei, L., Nurul Hasyimah Mohd Amin, I., & Raslan, R. (2011). Atomic force microscopy as a tool for asymmetric polymeric membrane characterization. *Sains Malaysiana, 40*(3), 237–244.

Mohammad, A. W., Ng, C. Y., Lim, Y. P., & Ng, G. H. (2012). Ultrafiltration in food processing industry: review on application, membrane fouling, and fouling control. *Food and Bioprocess Technology, 5*(4), 1143–1156. https://doi.org/10.1007/s11947-012-0806-9.

Mulder, M. (1996). *Basic principles of membrane technology* (2nd ed.). The Netherlands: Kluwer Academic Publishers.

Naidenko, E. S., Yukhin, Y. M., Afonina, L. I., & Gerasimov, K. B. (2012). Obtaining bismuth-potassium citrate. *Chemistry for Sustainable Development, 20*, 523–528.

Navarro, P., Perez-Lopez, A. J., Mercader, M. T., Carbonell-Barrachina, A. A., & Gabaldon, J. A. (2011). Antioxidant activity, color, carotenoids composition, minerals, vitamin C and sensory quality of organic and conventional mandarin juice cv. Orogrande. *Food Science and Technology International, 17*(3), 241–248. https://doi.org/10.1177/1082013210382334.

Nguyen, L. A. T., Schwarze, M., & Schomäcker, R. (2015). Adsorption of non-ionic surfactant from aqueous solution onto various ultrafiltration membranes. *Journal of Membrane Science, 493*(Supplement C), 120–133. https://doi.org/10.1016/j.memsci.2015.06.026.

Nyam, K. L., Tan, C. P., Lai, O. M., Long, K., & Che Man, Y. B. (2011). Optimization of supercritical CO_2 extraction of phytosterol-enriched oil from Kalahari melon seeds. *Food and Bioprocess Technology, 4*(8), 1432–1441. https://doi.org/10.1007/s11947-009-0253-4.

Odvina, C. V. (2006). Comparative value of orange juice versus lemonade in reducing stone-forming risk. *Clinical Journal of the American Society of Nephrology, 1*(6), 1269–1274. https://doi.org/10.2215/CJN.00800306.

Okino Delgado, C. H., & Fleuri, L. F. (2016). Orange and mango by-products: agro-industrial waste as source of bioactive compounds and botanical versus commercial description—a review. *Food Reviews International, 32*(1), 1–14. https://doi.org/10.1080/87559129.2015.1041183.

Pap, N., Mahosenaho, M., Pongrácz, E., Mikkonen, H., Jaakkola, M., Virtanen, V., Myllykoski, L., Horváth-Hovorka, Z., Hodúr, C., Vatai, G., & Keiski, R. L. (2012). Effect of ultrafiltration on anthocyanin and flavonol content of black currant juice (Ribes nigrum L.). *Food and Bioprocess Technology, 5*(3), 921–928. https://doi.org/10.1007/s11947-010-0371-z.

Pihlajamäki, A., Väisänen, P., & Nyström, M. (1998). Characterization of clean and fouled polymeric ultrafiltration membranes by Fourier transform IR spectroscopy–attenuated total reflection. *Colloids and Surfaces. A, Physicochemical and Engineering Aspects, 138*(2), 323–333. https://doi.org/10.1016/S0927-7757(96)03883-6.

Piironen, V., Toivo, J., Puupponen-Pimiä, R., & Lampi, A.-M. (2003). Plant sterols in vegetables, fruits and berries. *Journal of the Science of Food and Agriculture, 83*(4), 330–337. https://doi.org/10.1002/jsfa.1316.

Sagu, S. T., Karmakar, S., Nso, E. J., Kapseu, C., & De, S. (2014). Ultrafiltration of banana (Musa acuminata) juice using hollow fibers for enhanced shelf life. *Food and Bioprocess Technology, 7*(9), 2711–2722. https://doi.org/10.1007/s11947-014-1309-7.

Sass-Kiss, A., & Sass, M. (2000). Immunoanalytical method for quality control of orange juice products. *Journal of Agricultural and Food Chemistry, 48*(9), 4027–4031.

Sathishkumar, T., & Baskar, R. (2014). Screening and quantification of phytochemicals in the leaves and flowers in the leaves and flowers of Tabernaemontana heyneana Wall. *Indian Journal of Natural Products and Resources, 5*(3), 237–243.

Schmutzer, G. R., Dehelean, A., Magdas, D. A., Cristea, G., & Voica, C. (2016). Determination of stable isotopes, minerals, and volatile organic compounds in Romanian orange juice. *Analytical Letters, 49*(16), 2644–2658. https://doi.org/10.1080/00032719.2015.1130713.

Shahzad, N., Khan, W., Md, S., Ali, A., Saluja, S. S., Sharma, S., et al. (2017). Phytosterols as a natural anticancer agent: current status and future perspective. *Biomedicine & Pharmacotherapy, 88*(Supplement C), 786–794. https://doi.org/10.1016/j.biopha.2017.01.068.

Stinco, C. M., Fernández-Vázquez, R., Escudero-Gilete, M. L., Heredia, F. J., Meléndez-Martínez, A. J., & Vicario, I. M. (2012). Effect of orange juice's processing on the color, particle size, and bioaccessibility of carotenoids. *Journal of Agricultural and Food Chemistry, 60*(6), 1447–1455. https://doi.org/10.1021/jf2043949.

Tolve, R., Condelli, N., Can, A., & Tchuenbou-Magaia, F. L. (2018). Development and characterization of phytosterol-enriched oil microcapsules for foodstuff application. *Food and Bioprocess Technology, 11*(1), 152–163. https://doi.org/10.1007/s11947-017-1990-4.

Wang, M., Huang, W., Hu, Y., Zhang, L., Shao, Y., Wang, M., Zhang, F., Zhao, Z., Mei, X., Li, T., Wang, D., Liang, Y., Li, J., Huang, Y., Zhang, L., Xu, T., Song, H., Zhong, Y., & Lu, B. (2018). Phytosterol profiles of common foods and estimated natural intake of different structures and forms in China. *Journal of Agricultural and Food Chemistry, 66*(11), 2669–2676. https://doi.org/10.1021/acs.jafc.7b05009.

Weis, A., Bird, M. R., & Nyström, M. (2003). The chemical cleaning of polymeric UF membranes fouled with spent sulphite liquor over multiple operational cycles. *Journal of Membrane Science, 216*(1), 67–79. https://doi.org/10.1016/S0376-7388(03)00047-4.

Weis, A., Bird, M. R., Nyström, M., & Wright, C. (2005). The influence of morphology, hydrophobicity and charge upon the long-term performance of ultrafiltration membranes fouled with spent sulphite liquor. *Desalination, 175*(1), 73–85. https://doi.org/10.1016/j.desal.2004.09.024.

Wu, D., & Bird, M. R. (2007). The fouling and cleaning of ultrafiltration membranes during the filtration of model tea component solutions. *Journal of Food Process Engineering, 30*(3), 293–323. https://doi.org/10.1111/j.1745-4530.2007.00115.x.

Yang, M., Huang, F., Liu, C., Zheng, C., Zhou, Q., & Wang, H. (2013). Influence of microwave treatment of rapeseed on minor components content and oxidative stability of oil. *Food and Bioprocess Technology, 6*(11), 3206–3216. https://doi.org/10.1007/s11947-012-0987-2.

Yilmaz, E., & Bagci, P. O. (2019). Ultrafiltration of broccoli juice using Polyethersulfone membrane: Fouling analysis and evaluation of the juice quality. *Food and Bioprocess Technology, 12*(8), 1273–1283. https://doi.org/10.1007/s11947-019-02292-0.